THE JOURNAL OF PHYSICAL CHEMISTRY C

Article

Cite This: J. Phys. Chem. C 2019, 123, 12556−12562

pubs.acs.org/JPCC

Quantum and Phonon Interference-Enhanced Molecular-Scale Thermoelectricity

Hatef Sadeghi*

Physics Department, Lancaster University, Lancaster LA1 4YB, U.K.

Supporting Information

ABSTRACT: Simultaneous engineering of electron and phonon transport through nanoscale molecular junctions is fundamental to the development of high-performance thermoelectric materials for the conversion of waste heat into electricity and cooling. Here, we demonstrate a systematic improvement of the room-temperature thermoelectric figure of merit (ZT) of molecular junctions. This is achieved by phonon interference (PI)-suppressed thermal conductance and quantum interference-enhanced electrical conductance and Seebeck coefficient. This strategy leads to a significant enhancement of ZT from low values ca. 10^{-6} in oligo(phenylene-ethynylene) (OPE2) to the record values of 2.4 in dinitro-functionalized OPE2 (DOPE2). The dinitro functionalization also considerably enhances ZT of biphenyl-dithiol (BDT) and bipyridyl molecular junctions. Remarkably, the energy levels of electron-withdrawing nitro groups are hardly changed from one molecule to the other. Because of this generic feature, a resonance transport in the vicinity of Fermi energy of electrodes is formed leading to a significant improvement of Seebeck coefficient and ZT of all derivatives. For example, the Seebeck coefficient enhances from 10.8 μV/K in BDT to −470 μV/K in dinitro-BDT (DBDT). In addition, destructive PI due to the nitro groups suppresses phonon thermal conductance, for example, from 20 pW/K in BDT to 11 pW/K in DBDT at room temperature. We also demonstrate that quantum and PI-enhanced single-molecule thermoelectric efficiency is conserved when parallel molecules are placed between gold electrodes. These results promise to remove the key roadblocks and open new avenues to exploit functionalized organic molecules for thermoelectric energy harvesting and cooling.

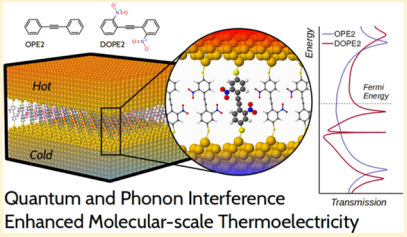

INTRODUCTION

Currently nearly 10% of the world's electricity is used by computers and the internet. This is expected to double over the next decade. Most of this energy is converted to heat. This waste heat could be used to generate electricity economically, provided materials with a high thermoelectric efficiency could be identified.[1] Conversely, efficient Peltier cooling using such materials would have applications to on-chip cooling of CMOS-based devices.[1] The demand for new thermoelectric materials has led to a worldwide race to develop materials with a high thermoelectric efficiency.[2] The efficiency of a thermoelectric device for power generation is characterized by the dimensionless figure of merit[3] $ZT = GS^2T/\kappa$, where G is the electrical conductance, S is the Seebeck coefficient (thermopower), T is temperature, and $\kappa = \kappa_{el} + \kappa_{ph}$ is the thermal conductance[4] due to electrons κ_{el} and phonons κ_{ph}. Therefore, low-κ, high-G, and high-S materials are needed for efficient conversion of heat into electricity. However, the interdependency of transport coefficients constrains the options for materials design and makes optimization a difficult task.

Despite several decades of development, the world record for ZT is only slightly above 2 at 900 K[5] and close to unity at room temperature,[6] which is not sufficient to create a viable technology platform. At the level of fundamental science, it was demonstrated recently that molecular wires can mediate long-range phase-coherent tunneling with remarkably low attenuation over sub-nanometer distances even at room temperature.[7] This creates the possibility of using quantum interference (QI) in single- or few-molecular junctions[8−11] to engineer enhancement of thermoelectricity in molecular materials[12,13] and design new high-performance organic materials.[14−16] The aim of this paper is to demonstrate that room-temperature QI (RTQI) of electrons can be employed to obtain high-G, high-S materials, and simultaneously room-temperature phonon interference (RTPI) can be used to suppress phonon thermal transport.

In this paper, we systematically characterize thermoelectric properties of biphenyl-dithiol (BDT), oligo(2-phenylene ethynylene) (OPE2) and bipyridine (BP)-based single molecule junctions. BDT, OPE2, and BP derivatives are placed between two hot and cold gold electrodes (Figure 1a; see Figure S1 of the Supporting Information for the optimized geometry of these molecules). BDT, OPE2, and BP molecules are ideal choices because they can be functionalized.[2,17−19] In addition, the electrical conductance and Seebeck coefficient measurement of parent BDT[20−22] and BP[23,24] molecules can be used for benchmarking. In what follows, our aim is to demonstrate for the first time that the thermoelectric efficiency of parent BDT, OPE2, and BP molecules is enhanced

Received: December 29, 2018
Revised: April 21, 2019
Published: May 14, 2019

DOI: 10.1021/acs.jpcc.8b12538
J. Phys. Chem. C 2019, 123, 12556−12562

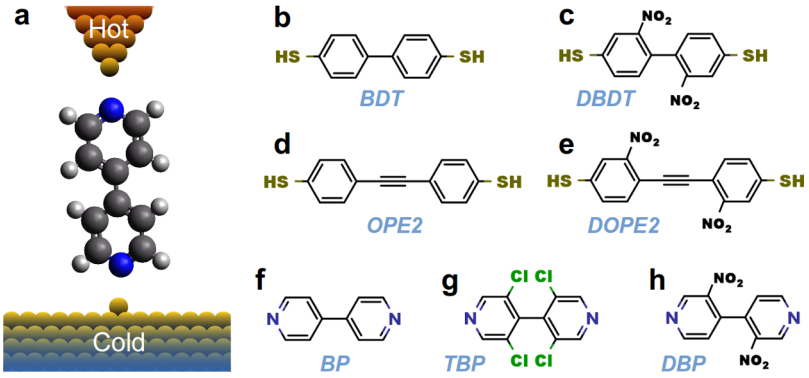

Figure 1. Thermoelectric molecular junction. (a) Molecular junction consists of bipyridine molecule between hot top and cold bottom electrodes. Molecular structure of (b) biphenyl-4,4′-dithiol BDT (c) 2,2′-dinitro-biphenyl-4,4′-dithiol DBDT (d) oligo(2-phenylene-4,4′-ethynylene)-dithiol OPE2, (e) 2,2′-dinitro-oligo(2-phenylene-4,4′-ethynylene)-dithiol DOPE2, (f) 4,4′-bipyridyl BP, (g) 3,3′,5,5′-tetrachloride-BP TBP and (h) 3,3′-dinitro-BP DBP. These molecules are viable synthetic target.

significantly by a systematic functionalization of their molecular structure.

We show that by introducing nitro (NO_2) side groups to BDT to form 2,2′-dinitro-BDT (DBDT), both Seebeck coefficient, and conductance enhance significantly. This is because electron-withdrawing nitro side groups form a resonance transport in the vicinity of Fermi energy of the electrode and in the gap of parent BDT. In addition, the thermal conductance due to phonons decreases considerably in the presence of nitro groups. Simultaneous RTQI enhancement of G and S and RTPI suppression of κ_{ph} lead to a high ZT. We also demonstrate that formation of resonance transport close to Fermi energy is a generic feature of molecules functionalized with nitro groups as evident in three different backbones, BDT, OPE2, and BP. Remarkably, the energy levels of nitro groups are hardly changed from one molecule to the other. This generic effect leads to a larger enhancement of thermoelectric efficiency in the vicinity of Fermi energy for molecules in which the electron transport is mainly through the highest occupied molecular orbital (HOMO). Nitro side groups enhance room temperature ZT of OPE2-dithiol molecular junctions from 4×10^{-6} to record values of 1.55 and 2.4. Chlorine side groups strongly suppress phonon transport through BP and enhance ZT. Furthermore, we show that RTQI and RTPI enhanced thermoelectricity is conserved when multiple parallel molecules are placed between electrodes. These results are significant because they open new avenues to exploit functionalized organic molecules for thermoelectric energy harvesting and cooling.

RESULTS AND DISCUSSION

From optimized geometry of the junctions, we obtain material-specific mean-field Hamiltonians using density functional theory (DFT). We then combine the obtained Hamiltonians with our transport code Gollum,[3,25] to calculate transmission coefficient $T_{el}(E)$ for electrons traversing from the hot electrode to the cold one (Figure 1a) through the molecules (see the Computational Methods section). $T_{el}(E)$ is combined with Laundauer formula to obtain the electrical conductance. In the low temperatures, the conductance $G = G_0 T_{el}(E_F)$ where G_0 is quantum conductance and E_F is the Fermi energy of electrodes. At room temperature, the conductance is obtained by thermal averaging of transmission coefficient weighted by the Fermi function (see the Computational Methods section).

Figure 2a shows the transmission coefficient of BDT derivatives. Transport through the biphenyl-4,4′-dithiol (BDT) molecule is mainly through the HOMO in agreement with the previous reports.[20−22] The measured conductance of parent BDT[22,26] is in the range of 3 to 7.5×10^{-3} G_0 in agreement with our calculation shown in Figure 2a for a wide range of energy around DFT Fermi energy ($E_F = 0$). The electronic thermal conductance κ_{el} and Seebeck coefficient S can also be calculated from $T_{el}(E)$ (see the Computational Methods section). Figure 2b,c shows κ_{el} and S for a range of energies around the DFT Fermi energy at room temperature. At $E_F = 0$, we obtain $S = 10.8$ μV/K and $\kappa_{el} = 2.3$ pW/K for BDT. Our calculated S is in agreement with measured values of 8.35 ± 0.23 μV/K.[22]

While experimental methods for measuring S of a single molecule using scanning-probe techniques are now rather well established, no such method exists for determining ZT of a single molecule because of difficulties in measuring the thermal

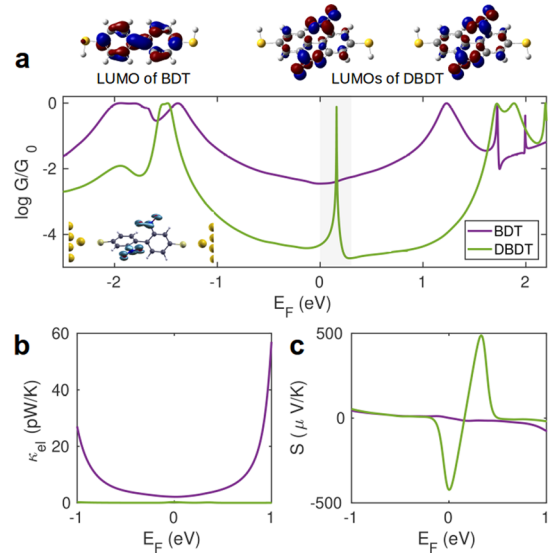

Figure 2. Electronic properties of the BDT-based molecular junctions. (a) Electron transmission coefficient vs energy, (b) room temperature electronic thermal conductance and (c) Seebeck coefficient vs Fermi energy of BDT and DBDT. Inset of (a) shows the local density of states on the DBDT for the energy range marked by gray color in (a) which includes the resonance.

DOI: 10.1021/acs.jpcc.8b12538
J. Phys. Chem. C 2019, 123, 12556−12562

conductance.[27,28] However, using material-specific ab initio calculation, we can calculate the phonon transmission coefficient $T_{ph}(\hbar\omega)$ of phonons with energy $\hbar\omega$ traversing from one electrode to the other. Using Laundauer-like formula, the thermal conductance due to phonons (κ_{ph}) is obtained from $T_{ph}(\hbar\omega)$ (see the Computational Methods section). Figure 3a,b show the phonon transmission coefficient $T_{ph}(\hbar\omega)$ and corresponding κ_{ph} for BDT molecule. We predict κ_{ph} = 19.6 pW/K for BDT molecular junction which is 5 times higher than room temperature κ_{el}. This means that the thermal conductance is dominated by phonons in this junction. A low S and high κ in BDT, leads to a low-room temperature $ZT = 5 \times 10^{-4}$ (Figure 3c) at the Fermi energy. In what follows, we demonstrate that high values of ZT can be obtained in nitro-functionalized BDT (DBDT) which is driven by RTQI and RTPI effects.

The molecular structure of DBDT is shown in Figure 1c where two hydrogen atoms in BDT are replaced by two NO_2 groups. The electronic transmission coefficient is shown in Figure 2a. The amplitude of $T_{el}(E)$ decreases except around the Fermi energy where a resonance is formed. Local density of state calculations (inset of Figure 2a) for energy range around the resonance (marked by the gray region in Figures 2a and S2a of the Supporting Information) and lowest unoccupied molecular orbital (LUMO) of gas phase BDT and DBDT (Figure S2a and Table S2 of the Supporting Information) confirms that this resonance is due to the localized states on NO_2 groups. Because of the interference[3] between transmitted wave through the backbone and reflected wave by nitro groups, a Fano resonance is formed. On one hand, because of the steric hindrance of nitro side groups, the two benzene rings are rotated and form an angle of 77.8°. This reduces the overlap between p orbitals[29] and decreases the conductance for a wide range of energies in DBDT compared to parent BDT (Figure 2a). On the other hand, because of the resonance close to the Fermi energy, the conductance increases in DBDT compared to parent BDT around E_F. In addition, S is improved significantly to ca. −470 μV/K in DBDT compared to that of parent BDT (S = 10.8 μV/K). This is due to a high slope of transmission coefficient close to this resonance (Figure 2c). S is proportional to the slope of natural logarithm of the transmission coefficient $T_{el}(E)$ evaluated at the Fermi energy ($S \propto \partial \ln T(E)/\partial E$ at $E = E_F$).[3]

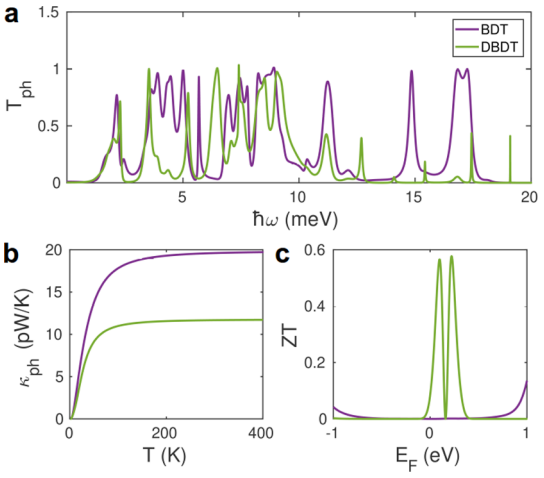

Figure 3. Phononic properties of the BDT-based molecular junctions and thermoelectric figure of merit. (a) Phonon transmission coefficient vs energy and LUMO states of BDT and DBDT, (b) phononic thermal conductance vs temperature and (c) room temperature ZT vs Fermi energy of BDT, and DBDT.

Furthermore, by introducing NO_2 side groups to BDT, $T_{ph}(\hbar\omega)$ suppresses in DBDT (Figure 3a) and κ_{ph} decreases strongly (Figure 3b). Just like a guitar string where waves with certain frequencies are suppressed by pressing the string, introducing a heavy side group suppresses phonons with given frequencies. The side groups with higher mass supress lower frequency modes. Our calculation shows that the room-temperature thermal conductance of DBDT (κ_{ph} = 11.7 pW/K) is about two times lower than that of parent DBT. QI-mediated high-G and high-S is combined with the PI-mediated suppression of κ to yield a significant improvement of ZT from ca. 10^{-4} in parent DBT to ca. 0.55 in DBDT in the vicinity of the Fermi energy (Figure 3c).

To demonstrate that enhancement of ZT due to the nitro side groups is independent of the molecular backbone, we study thermoelectric properties of OPE2 derivatives (Figures 1d,e and 5a–d). Figure 4a shows the electron transmission coefficient through OPE2 and its nitro-functionalized derivative DOPE2. The electrical conductance of OPE2 single-molecule junction is about 0.6×10^{-3} (Figure 4a) at the DFT Fermi energy in agreement with the reported experimental values.[30] OPE2 is a fully conjugated molecule and its ground-state structure is planar. Unlike DBDT, where the two benzene rings were rotated because of the steric hindrance of two close NO_2 groups, DOPE2 remains planar because the rings are separated by ethynylene groups and are far from each other. Therefore, the conductance reduction in DBDT is not present in DOPE2 (see Figure S14 of the Supporting Information).

By nitro functionalization, two new states are formed in the HOMO–LUMO gap of the parent OPE2 (Figure 4b) which are mainly localized on the nitro groups. Consequently, two new resonances in $T_{el}(E)$ of DOPE2 are formed in the HOMO–LUMO gap of the parent OPE2 (Figure 4a). The local density of state calculation in the vicinity of these resonances (Figure S3 of the Supporting Information) also confirms that these resonances are due to nitro groups. The new LUMO resonance close to the DFT Fermi energy leads to a simultaneous enhancement of G and S. Electrical conductance increases from ca. 0.6×10^{-3} in OPE2 to ca. 10^{-2} in DOPE2 (Figure 4a). S also increases from ca. 6 μV/K in OPE2 to ca. −180 μV/K in DOPE2 (Figure 4b). Phonon transmission through DOPE2 is suppressed for lower frequencies because of nitro groups (Figure S5a of the Supporting Information) but it increases for higher energy phonons. Therefore, κ_{ph} of OPE2 (9.9 pW/K) and DOPE2 (9.7 pW/K) remains almost the same (Figure S5 of the Supporting Information). High-G and high-S in DOPE2 lead to a significant enhancement of the full ZT from 5×10^{-6} in OPE2 to a record value of 1.55 in DOPE2 at room temperature (Figure 4c). This is even increased further to 2.4 by a few meV shift of E_F.

To understand the effect of nitro group on electron transport, we note that the transmission coefficient through a one-level system with energy ε_0 in the presence of a pendent group with energy ε_p between two 1D leads (Figure S9 of the Supporting Information) is obtained from Breit–Wigner formula:[3] $T_{el}(E) = 4\Gamma_L\Gamma_R/((E - \varepsilon_n)^2 + (\Gamma_L + \Gamma_R)^2)$ where $\varepsilon_n = \varepsilon_0 - \sigma + a^2/(E - \varepsilon_p)$, $\Gamma_{L,R}$ are tunnel rates and λ is the eigen energy of the molecular orbital shifted slightly by an amount σ because of the coupling of the orbital to the

DOI: 10.1021/acs.jpcc.8b12538
J. Phys. Chem. C 2019, 123, 12556–12562

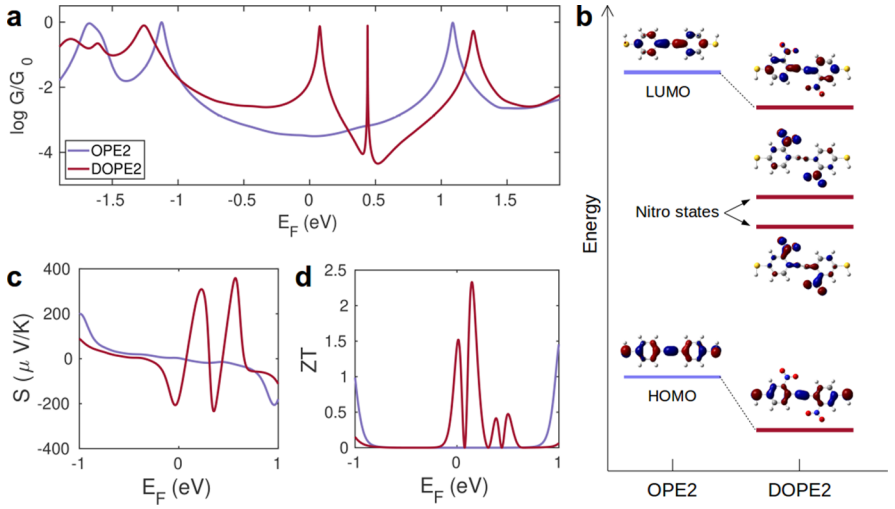

Figure 4. Thermoelectric properties of the OPE2-based molecular junctions. (a) Electron transmission coefficient vs energy, room temperature, (b) frontier orbitals of OPE2 and DOPE2. Seebeck coefficient S (c) and total thermoelectric figure of merit ZT (d) vs Fermi energy of OPE2 and DOPE2.

electrodes. If an electron resonates with the molecular orbital ($E = \varepsilon_n$), electron transmission is a maximum, whereas electron transmission is destroyed at $E = \varepsilon_p$. This antiresonance at $E = \varepsilon_p$ followed by a resonance at $E = \varepsilon_n$ called Fano resonance. The width of Fano resonance is proportional to the coupling between the orbital and the pendent group. The energy of nitro groups are close to the DFT Fermi energy, therefore, Fano resonance happens to be around E_F. Two Fano resonances are expected because of two nitro groups with the same energy. The splitting between these two degenerate states depends on the indirect coupling between them through the backbone of DBDT and DOPE2. Because two rings are coupled to each other stronger in DOPE2 compare to that of DBDT, two resonances (LUMO and LUMO + 1 in Figure 4a) are formed in transmission coefficient of DOPE2. By moving the intro groups in DOPE2 from ortho to meta positions to form DOPE2-m (Figure 5a), the electronic coupling between NO_2 groups through the backbone decreases dramatically.

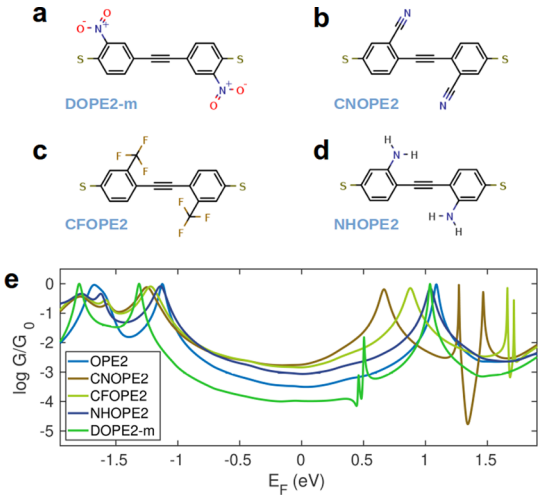

Figure 5. OPE2 derivatives. OPE2 with different side groups (a) NO_2 in meta position, (b) CN, (c) CF_3, (d) NH_2. (e) Electron transmission coefficient for OPE2 derivatives between two gold electrodes.

This is because the effective electronic coupling between two sites in a molecule is proportional to Green's function matrix element between the two sites as demonstrated in the Supporting Information. In the vicinity of the middle of the HOMO−LUMO gap, Green's function matrix element between the meta sites is smaller than that of the ortho sites because of a destructive QI of standing waves. Consequently, the splitting of the resonances due to the nitro groups is smaller in DOPE2-m compared to that of DOPE2 (Figures 5e and 6a). This is also demonstrated with a simple tight-binding model in the Supporting Information (see Figure S10).

Because nitro is a strong electron-withdrawing group, we have studied the effect of another electron-withdrawing group,

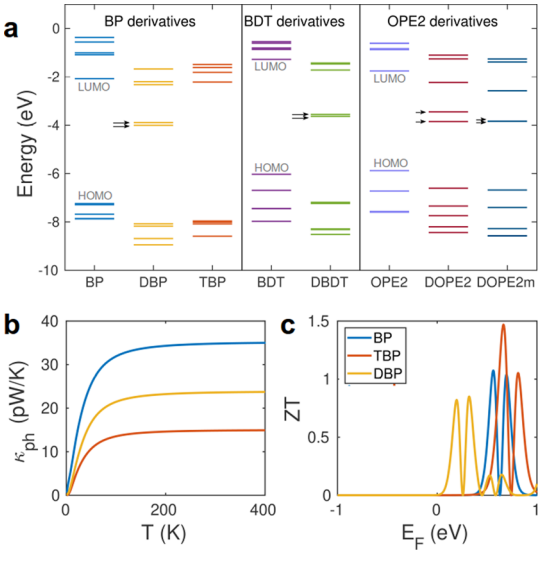

Figure 6. Energy level diagram of gas phase BP, BDT, and OPE2 derivatives and thermoelectric properties of the BP-based molecular junctions. (a) Energy levels of gas phase molecules calculated using B3LYP functional (see the Computational Methods section). Two degenerate energy levels around −4 eV are mainly due to the nitro group as evident by their associated wave functions in Tables S1−S3. (b) Phonon thermal conductance and (c) room temperature ZT vs Fermi energy of BP, TBP, and DBP junctions.

DOI: 10.1021/acs.jpcc.8b12538
J. Phys. Chem. C 2019, 123, 12556−12562

cyano (CN) on transport properties of OPE2 as shown in Figure 5b. As a result of cyano functionalization of OPE2 (to form CNOPE2), the LUMO resonance moves toward the Fermi energy (Figure 5e and Tables S3 and S4 of the Supporting Information). The wave function calculations of gas phase CNOPE2 reveals that the state due to the CN group hybridizes with the LUMO of OPE2 backbone and forms a new LUMO state closer to the Fermi energy (Table S4 of the Supporting Information). We did not find a sizable effect on the transport properties of OPE2 using other functionalization such as CF_3 and NH_2 (Figure 5c−e and Table S4 of the Supporting Information).

To examine the effect of side groups on the thermoelectric properties of BP derivatives, we study electron and phonon transport through 4,4′-bipyridyl (BP), 3,3′,5,5′-tetrachloride-BP (TBP) and 3,3′-dinitro-BP (DBP) molecules shown in Figure 1d−f. Figure S6a shows the transmission coefficient of BP derivatives. Transport through the BP molecule is mainly through LUMO in agreement with the previous reports.[23,31] The measured conductance of the BP molecule[23,32] is in the range of 0.9 to 4.4×10^{-4} G_0 in agreement with our calculation (Figure S6a) for a wide range of energies around $E = 0$ eV.

Our calculation shows that the electron transport is also mainly through LUMO in TBP and DBP functionalized molecular junctions. Their conductances are smaller than BP parent at E_F (Figure S6a). This is because of the rotation of two pyridine rings relative to each other in TBP and DBP (see Figure S1 of the Supporting Information). The conductance is expected to reduce by $\cos(\theta)$ where θ is the angle between pyridine rings.[29] θ is 66° and 79° in TBP and DBP, respectively. Our transport calculations (Figure S6a) show that the conductance of the DBP junction is smaller than that of TBP. Just like DOPE2 and DBDT molecular junctions where a resonance due to NO_2 side groups is formed between HOMO and LUMO of parent OPE2 and BDT, the resonance in $T_{el}(E)$ of DBP is formed between HOMO and LUMO of BP (Figure S6a). Figure 6a shows the energy levels of gas-phase BP, BDT, and OPE2 derivatives. Remarkably, two degenerate energy levels (indicated by black arrows in Figure 6a) are located about $E = -4$ eV for all nitro functionalized molecules. As illustrated with the wave function calculations of Tables S1−S3 of the Supporting Information, these states are localized on NO_2 groups.

Figure S6c of the Supporting Information shows S of BP, TBP, and DBP at room temperature. A negative Seebeck coefficient in the range of −7.9 to −9.5 μV/K is obtained for parent BP around E_F in agreement with previous measurements.[23,24] S of the functionalized DBP molecule is higher compared to that of BP and TBP around E_F. A few meV away from E_F, S of DBP increases to ca. −380 μV/K (Figure S6c). This tiny shift of E_F can be achieved by doping using charge-transfer complexes or electrostatic gating using a third electrode. By introducing side groups to BP, for example, Cl or NO_2, $T_{ph}(\hbar\omega)$, and κ_{ph} of TBP and DBP is suppressed (Figure S7b of the Supporting Information). Room temperature κ_{ph} of BP, TBP, and DBP are 34.8, 14.8 and 23.6 pW/K, respectively (Figure 6b). Although NO_2 side groups are heavier than Cl, κ_{ph} is supressed largely in TBP. This is because the number of side groups (4 chlorine atoms) in TBP is more than that of DBP with only two NO_2 side groups. Note that unlike the monotonic angle dependence of electronic transmission, dependence of phonon transmission to θ is non-monotonic (Figure 6b). By increasing θ, κ_{ph} decreases from BP to TBP, whereas it increases from TBP to DBP. In fact, phonon transmission is mainly influenced by the side groups not θ. Figure 6c shows the total ZT of BP derivatives. Clearly, ZT enhances from parent BP to nitro functionalized DBP. A larger improvement of room temperature $ZT = 0.9$ in DBP is possible at a few meV away from the Fermi energy. It is worth mentioning that the nitro-functionalization reduces phonon thermal conductance of all junctions. The main contribution to the total thermal conductance of all nitro-functionalized junctions is due to phonons except in DOPE2 where the improvement of electron transmission coefficient and consequently electron thermal conductance is larger than phonon contribution to the total thermal conductance.

To understand how the thermoelectric performance of molecular devices changes by up-scaling to many molecule junctions, we calculate the electronic and phononic properties of junctions formed with two BP molecules sandwiched between gold electrodes as shown in Figure S11 of the Supporting Information. The electron transmission coefficient increases by almost a factor of 2 for a wide range of energy between HOMO and LUMO (Figure S8a of the Supporting Information). S is nearly unchanged because the slope of electronic transmission coefficient does not change by the number of molecules (Figure S8c). Phonon transmission and κ_{ph} is almost scaled linearly with the number of molecules (Figure S8d,e of the Supporting Information). Consequently, ZT is hardly affected. Unlike junctions formed from graphene electrodes, where indirect coupling between molecules through the graphene electrodes lead to a QI and nonlinear variations of thermoelectric properties,[33] in the junctions formed by gold electrodes, interference effects due to indirect coupling is less significant provided there is not a direct coupling between molecules e.g. through cross-linking.

CONCLUSIONS

We have studied systematically the thermoelectric properties of BDT, oligo(2-phenylene ethynylene), and bipyridine derivatives. We calculated the electron and phonon transport from the first principle. Guided by quantum and phonon interference effects; we engineered the molecular structures and enhanced the thermoelectric efficiency. We showed that record values of $ZT = 1.55$ and 2.4 are accessible in the nitro-functionalized OPE2-ditihol molecules. Nitro groups also enhance ZT of BDT and BP derivatives. Energy level diagram of gas phase molecules shows that energy levels of nitro groups are moved hardly from one molecule to the other. This suggests that enhancement of ZT using nitro functionalization is a generic feature and is independent of the choice of a parent molecule. The enhancement of ZT by NO_2 groups is more significant in HOMO dominated DBDT and DOPE2-dithiol molecules. Furthermore, we showed that phonon transport can be suppressed strongly in tetrachloride-BP compared to its parent BP leading to enhancement of ZT. Unlike a monotonic dependence of electronic transmission of BP derivatives to angle between two pyridines, angle dependence of phonon transmission is nonmonotonic. We also demonstrated that in the junctions formed by gold electrodes, interference effects due to indirect couplings through the leads are less significant. Consequently, RTQI and RTPI enhanced ZT is conserved when parallel molecules are placed between gold electrodes.

DOI: 10.1021/acs.jpcc.8b12538
J. Phys. Chem. C 2019, 123, 12556−12562

COMPUTATIONAL METHODS

Geometry Optimization. The geometry of each structure was relaxed to the force tolerance of 10 meV/Å using the SIESTA[34] implementation of DFT, with a double-ζ-polarized basis set and the generalized gradient approximation functional with Perdew−Burke−Ernzerhof parameterization. A real-space grid was defined with an equivalent energy cutoff of 250 Ry. For energy level diagram (Figure 6a) and wave function calculations (Tables S1−S4 of the Supporting Information) of gas phase molecules, we employed experimentally parameterized B3LYP functional using Gaussian g09v2[35] with 6-311++g basis set and tight convergence criteria.

Phonon Transport. Following the method described in refs,[3,28] a set of *xyz* coordinates were generated by displacing each atom from the relaxed *xyz* geometry in the positive and negative *x*, *y*, and *z* directions with $\delta q' = 0.01$ Å. The forces $F_i^q = (F_i^x, F_i^y, F_i^z)$ in three directions $q_i = (x_i, y_i, z_i)$ on each atom were then calculated and used to construct the dynamical matrix $D_{ij} = K_{ij}^{qq'}/M_{ij}$ where the mass matrix $M = \sqrt{M_i M_j}$ and $K_{ij}^{qq'} = [F_i^q(\delta q_j') - F_j^q(-\delta q_j')]/2\delta q_j'$ for $i \neq j$ obtained from finite differences. To satisfy momentum conservation, the K for $i = j$ (diagonal terms) is calculated from $K_{ii} = -\sum_{i\neq j} K_{ij}$. The phonon transmission $T_{ph}(\omega)$ then can be calculated from the relation $T_{ph}(\omega) = \mathrm{Trace}(\Gamma_L^{ph}(\omega) G_{ph}^R(\omega) \Gamma_R^{ph}(\omega) G_{ph}^{R\dagger}(\omega))$ where $\Gamma_{L,R}^{ph}(\omega) = i(\sum_{L,R}^{ph}(\omega) - \sum_{L,R}^{ph\dagger}(\omega))$ describes the level broadening due to the coupling to the left L and right R electrodes, $\sum_{L,R}^{ph}(\omega)$ are the retarded self-frequencies associated with this coupling and $G_{ph}^R = (\omega^2 I - D - \sum_L^{ph} - \sum_R^{ph})^{-1}$ is the retarded Green's function, where D and I are the dynamical and the unit matrices, respectively. The phonon thermal conductance κ_{ph} at temperature T is then calculated from $\kappa_{ph}(T) = (2\pi)^{-1} \int_0^\infty \hbar\omega T_{ph}(\omega)(\partial f_{BE}(\omega,T)/\partial T) d\omega$ where $f_{BE}(\omega,T) = (e^{\hbar\omega/k_B T} - 1)^{-1}$ is Bose−Einstein distribution function and $\hbar$ is reduced Planck's constant and $k_B = 8.6 \times 10^{-5}$ eV/K is Boltzmann's constant.

Electron Transport. To calculate electronic properties of the device, from the converged DFT calculation, the underlying mean-field Hamiltonian H was combined with our quantum transport code, Gollum.[3,25] This yields the transmission coefficient $T_{el}(E)$ for electrons of energy E (passing from the source to the drain) via the relation $T_{el}(E) = \mathrm{Tr}(\Gamma_L^{el}(E) G_{el}^R(E) \Gamma_R^{el}(E) G_{el}^{R\dagger}(E))$ where $\Gamma_{L,R}^{el}(E) = i(\sum_{L,R}^{el}(E) - \sum_{L,R}^{el\dagger}(E))$ describes the level broadening due to the coupling between left L and right R electrodes and the central scattering region, $\sum_{L,R}^{el}(E)$ are the retarded self-energies associated with this coupling and $G_{el}^R = (ES - H - \sum_L^{el} - \sum_R^{el})^{-1}$ is the retarded Green's function, where H is the Hamiltonian and S is the overlap matrix obtained from SIESTA implementation of DFT. DFT + $\sum$ approach has been employed for spectral adjustment.[3]

Thermoelectric Properties. Using the approach explained in ref 3, the electrical conductance $G_{el}(T) = G_0 L_0$, the electronic contribution of the thermal conductance $\kappa_{el}(T) = (L_0 L_2 - L_1^2)/hTL_0$ and the thermopower $S(T) = -L_1/eTL_0$ are calculated from the electron transmission coefficient $T_{el}(E)$ where the moments $L_n(T) = \int_{-\infty}^{+\infty} dE(E - E_F)^n T_{el}(E)(-\partial f_{FD}(E,T)/\partial E)$ and $f_{FD}(E,T)$ is the Fermi-Dirac probability distribution function $f_{FD}(E,T) = (e^{(E-E_F)/k_B T} + 1)^{-1}$, T is the temperature, E_F is the Fermi energy, $G_0 = 2e^2/h$ is the conductance quantum, e is electron charge and h is the Planck's constant. The full thermoelectric figure of merit ZT is then calculated as $ZT(E_F,T) = G(E_F,T)S(E_F,T)^2 T/\kappa(E_F,T)$ where $G(E_F,T)$ is the electrical conductance, $S(E_F,T)$ is Seebeck coefficient, $\kappa(E_F,T) = \kappa_{el}(E_F,T) + \kappa_{ph}(T)$ is the thermal conductance due to the electrons and phonons, E_F is Fermi energy and T is temperature.

ASSOCIATED CONTENT

Supporting Information

The Supporting Information is available free of charge on the ACS Publications website at DOI: 10.1021/acs.jpcc.8b12538.

Additional DFT calculations, electron and phonon transmission functions for all molecules, gas phase molecular orbital calculations, and tight-binding model (PDF)

AUTHOR INFORMATION

Corresponding Author

*E-mail: h.sadeghi@lancaster.ac.uk and hatef.sadeghi@gmail.com.

ORCID

Hatef Sadeghi: 0000-0001-5398-8620

Notes

The author declares no competing financial interest.

ACKNOWLEDGMENTS

The author acknowledges the Leverhulme Trust for Early Career Fellowship no. ECF-2017-186 and UKRI Future Leaders Fellowship no. MR/S015329/1.

REFERENCES

(1) Disalvo, F. J. Thermoelectric Cooling and Power Generation. *Science* **1999**, *285*, 703−706.

(2) Reddy, P.; Jang, S.-Y.; Segalman, R. A.; Majumdar, A. Thermoelectricity in Molecular Junctions. *Science* **2007**, *315*, 1568−1571.

(3) Sadeghi, H. Theory of Electron, Phonon and Spin Transport in Nanoscale Quantum Devices. *Nanotechnology* **2018**, *29*, 373001.

(4) Sergueev, N.; Shin, S.; Kaviany, M.; Dunietz, B. Efficiency of Thermoelectric Energy Conversion in Biphenyl-Dithiol Junctions: Effect of Electron-Phonon Interactions. *Phys. Rev. B: Condens. Matter Mater. Phys.* **2011**, *83*, 195415.

(5) Zhao, L.-D.; Lo, S.-H.; Zhang, Y.; Sun, H.; Tan, G.; Uher, C.; Wolverton, C.; Dravid, V. P.; Kanatzidis, M. G. Ultralow Thermal Conductivity and High Thermoelectric Figure of Merit in SnSe Crystals. *Nature* **2014**, *508*, 373−377.

(6) Snyder, G. J.; Toberer, E. S. Complex Thermoelectric Materials. *Nat. Mater.* **2008**, *7*, 105−114.

(7) Sedghi, G.; García-Suárez, V. M.; Esdaile, L. J.; Anderson, H. L.; Lambert, C. J.; Martín, S.; Bethell, D.; Higgins, S. J.; Elliott, M.; Bennett, N.; et al. Long-Range Electron Tunnelling in Oligo-Porphyrin Molecular Wires. *Nat. Nanotechnol.* **2011**, *6*, 517−523.

(8) Sangtarash, S.; Huang, C.; Sadeghi, H.; Sorohhov, G.; Hauser, J.; Wandlowski, T.; Hong, W.; Decurtins, S.; Liu, S.-X.; Lambert, C. J. Searching the Hearts of Graphene-like Molecules for Simplicity, Sensitivity, and Logic. *J. Am. Chem. Soc.* **2015**, *137*, 11425−11431.

(9) Sadeghi, H.; Sangtarash, S.; Lambert, C. J. Electron and Heat Transport in Porphyrin-Based Singlemolecule Transistors with Electro-Burnt Graphene Electrodes. *Beilstein J. Nanotechnol.* **2015**, *6*, 1413−1420.

(10) Sadeghi, H.; Mol, J. A.; Lau, C.; Briggs, A.; Warner, J.; Lambert, C. J.; Siong, C.; Briggs, G. A. D.; Warner, J.; Lambert, C. J.; et al. Conductance Enlargement in Pico-Scale Electro-Burnt Graphene Nanojunctions. *Proc. Natl. Acad. Sci. U.S.A.* **2015**, *112*, 2658−2663.

(11) Sadeghi, H.; Sangtarash, S.; Lambert, C. J. Enhanced Thermoelectric Efficiency of Porous Silicene Nanoribbons. *Sci. Rep.* **2015**, *5*, 9514.

DOI: 10.1021/acs.jpcc.8b12538
J. Phys. Chem. C 2019, 123, 12556−12562

(12) Miao, R.; Xu, H.; Skripnik, M.; Cui, L.; Wang, K.; Pedersen, K. G. L.; Leijnse, M.; Pauly, F.; Wärnmark, K.; Meyhofer, E.; et al. Influence of Quantum Interference on the Thermoelectric Properties of Molecular Junctions. *Nano Lett.* **2018**, *18*, 5666−5672.
(13) Sangtarash, S.; Sadeghi, H.; Lambert, C. J. Connectivity-Driven Bi-Thermoelectricity in Heteroatom-Substituted Molecular Junctions. *Phys. Chem. Chem. Phys.* **2018**, *20*, 9630−9637.
(14) Su, T. A.; Neupane, M.; Steigerwald, M. L.; Venkataraman, L.; Nuckolls, C. Chemical Principles of Single-Molecule Electronics. *Nat. Rev. Mater.* **2016**, *1*, 16002.
(15) Platzman, I.; Haick, H.; Tannenbaum, R. Self-Assembly of Organic Monolayers as Protective and Conductive Bridges for Nanometric Surface-Mount Applications. *ACS Appl. Mater. Interfaces* **2010**, *2*, 2585−2593.
(16) Rincón-García, L.; Evangeli, C.; Rubio-Bollinger, G.; Agraït, N. Thermopower Measurements in Molecular Junctions. *Chem. Soc. Rev.* **2016**, *45*, 4285−4306.
(17) Li, B.; Zhang, Y.; Li, G.; Liu, D.; Chen, Y.; Hu, W.; Shi, Z.; Feng, S. Design and Construction of Coordination Polymers by 2,2′-Dinitro-4, 4′-Biphenyldicarboxylate and Imidazole-Based Ligands: Diverse Structures Based on Different Metal Ions. *CrystEngComm* **2011**, *13*, 2457.
(18) Lu, Q.; Liu, K.; Zhang, H.; Du, Z.; Wang, X.; Wang, F. From Tunneling to Hopping: A Comprehensive Investigation of Charge Transport Mechanism in Molecular Junctions Based on Oligo(p-Phenylene Ethynylene)S. *ACS Nano* **2009**, *3*, 3861−3868.
(19) Xin, N.; Guan, J.; Zhou, C.; Chen, X.; Gu, C.; Li, Y.; Ratner, M. A.; Nitzan, A.; Stoddart, J. F.; Guo, X. Concepts in the Design and Engineering of Single-Molecule Electronic Devices. *Nat. Rev. Phys.* **2019**, *1*, 211.
(20) Malen, J. A.; Doak, P.; Baheti, K.; Tilley, T. D.; Majumdar, A.; Segalman, R. A. The Nature of Transport Variations in Molecular Heterojunction Electronics. *Nano Lett.* **2009**, *9*, 3406−3412.
(21) Tan, A.; Balachandran, J.; Sadat, S.; Gavini, V.; Dunietz, B. D.; Jang, S. Y.; Reddy, P.; Jang, S. Y.; Reddy, P. Effect of Length and Contact Chemistry on the Electronic Structure and Thermoelectric Properties of Molecular Junctions. *J. Am. Chem. Soc.* **2011**, *133*, 8838−8841.
(22) Guo, S.; Zhou, G.; Tao, N. Single Molecule Conductance, Thermopower, and Transition Voltage. *Nano Lett.* **2013**, *13*, 4326−4332.
(23) Kim, T.; Darancet, P.; Widawsky, J. R.; Kotiuga, M.; Quek, S. Y.; Neaton, J. B.; Venkataraman, L.; Junctions, S.; Kim, T.; Darancet, P.; et al. Determination of Energy Level Alignment and Coupling Strength in 4,4′-Bipyridine Single-Molecule Junctions. *Nano Lett.* **2014**, *14*, 794−798.
(24) Widawsky, J. R.; Darancet, P.; Neaton, J. B.; Venkataraman, L. Simultaneous Determination of Conductance and Thermopower of Single Molecule Junctions. *Nano Lett.* **2012**, *12*, 354−358.
(25) Ferrer, J.; Lambert, C. J.; García-Suárez, V. M.; Manrique, D. Z.; Visontai, D.; Oroszlany, L.; Rodríguez-Ferradás, R.; Grace, I.; Bailey, S. W. D.; Gillemot, K.; et al. GOLLUM: A next-Generation Simulation Tool for Electron, Thermal and Spin Transport. *New J. Phys.* **2014**, *16*, 093029.
(26) Kim, Y.; Jeong, W.; Kim, K.; Lee, W.; Reddy, P. Electrostatic Control of Thermoelectricity in Molecular Junctions. *Nat. Nanotechnol.* **2014**, *9*, 881−885.
(27) Meier, T.; Menges, F.; Nirmalraj, P.; Hölscher, H.; Riel, H.; Gotsmann, B. Length-Dependent Thermal Transport along Molecular Chains. *Phys. Rev. Lett.* **2014**, *113*, 060801.
(28) Sadeghi, H.; Sangtarash, S.; Lambert, C. J. Oligoyne Molecular Junctions for Efficient Room Temperature Thermoelectric Power Generation. *Nano Lett.* **2015**, *15*, 7467−7472.
(29) Venkataraman, L.; Klare, J. E.; Nuckolls, C.; Hybertsen, M. S.; Steigerwald, M. L. Dependence of Single-Molecule Junction Conductance on Molecular Conformation. *Nature* **2006**, *442*, 904−907.
(30) Kaliginedi, V.; Moreno-García, P.; Valkenier, H.; Hong, W.; García-Suárez, V. M.; Buiter, P.; Otten, J. L. H.; Hummelen, J. C.; Lambert, C. J.; Wandlowski, T. Correlations between Molecular Structure and Single Junction Conductance: A Case Study with OPE-Type Wires. *J. Am. Chem. Soc.* **2012**, *134*, 5262−5275.
(31) Bagrets, A.; Arnold, A.; Evers, F. Conduction Properties of Bipyridinium-Functionalized Molecular Wires. *J. Am. Chem. Soc.* **2008**, *130*, 9013−9018.
(32) Quek, S. Y.; Kamenetska, M.; Steigerwald, M. L.; Choi, H. J.; Louie, S. G.; Hybertsen, M. S.; Neaton, J. B.; Venkataraman, L. Mechanically Controlled Binary Conductance Switching of a Single-Molecule Junction. *Nat. Nanotechnol.* **2009**, *4*, 230−234.
(33) Wu, Q.; Sadeghi, H.; García-Suárez, V. M.; Ferrer, J.; Lambert, C. J. Thermoelectricity in Vertical Graphene-C60-Graphene Architectures. *Sci. Rep.* **2017**, *7*, 11680.
(34) Soler, J. M.; Artacho, E.; Gale, J. D.; García, A.; Junquera, J.; Ordejón, P.; Sánchez-Portal, D. The SIESTA Method for Ab Initio Order-N Materials Simulation. *J. Phys.: Condens. Matter* **2002**, *14*, 2745−2779.
(35) Frisch, M. J. *Gaussian G9*; Gaussian, Inc.: Wallingford CT, 2016.

DOI: 10.1021/acs.jpcc.8b12538
J. Phys. Chem. C 2019, 123, 12556−12562